Hindawi
International Journal of Aerospace Engineering
Volume 2019, Article ID 6024240, 13 pages
https://doi.org/10.1155/2019/6024240

Research Article

Nonsingular Continuous Finite-Time Convergent Guidance Law with Impact Angle Constraints

Luyao Zang,[1,2] **Defu Lin**,[1,2] **and Yi Ji**[1,2]

[1]*School of Aerospace Engineering, Beijing Institute of Technology, 5th Zhongguancun South Street, Beijing 100081, China*
[2]*Beijing Key Laboratory of UAV Autonomous Control, Beijing Institute of Technology, 5th Zhongguancun South Street, Beijing 100081, China*

Correspondence should be addressed to Luyao Zang; luyao_jizi@126.com

Received 15 December 2018; Accepted 3 February 2019; Published 7 April 2019

Academic Editor: Mahmut Reyhanoglu

This paper documents a novel nonsingular continuous guidance which can drive the line-of-sight (LOS) angular rate to converge to zero in finite time in the presence of impact angle constraints. More specifically, based on the second-order sliding mode control (SMC) theory, a second-order observer (2-OB) is presented to estimate the unknown target maneuvers, while a super twisting algorithm- (STA-) based guidance law is presented to restrict the LOS angle and angular rate. Compared with other terminal sliding mode guidance laws, the proposed guidance law absorbs the merits of the conventional linear sliding mode (LSM) and terminal sliding mode (TSM) and uses switching technique to avoid singularity. In order to verify the stability of the proposed guidance law, a finite-time bounded (FTB) function is invited to prove the boundedness of the proposed observer-controller system and a Lyapunov approach is presented to prove the finite-time convergence (FTC) of the proposed sliding system. Rigorous theoretical analysis and numerical simulations demonstrate the mentioned properties.

1. Introduction

Facing the modern battleground, zero miss distance is not the only operational effect index of accurately guided weapon guidance [1]. The complex combat circumstance requires some new properties, such as energy optimization, interference resistance, and impact angle constraints. Among these requirements, impact angle constraints are one of the prerequisites for some real cases. For example, for a missile against a tank, it is easy to pierce the top rather than the armored body; this process requires that the missile intercepts the tank within a limited impact angle range that can be realized by using a reasonable guidance law design.

Because of their effectiveness, ease of implementation, and successful history of application, the well-known proportional navigation guidance (PNG) law [2–5] and its variants have been widely used in engineering practice in the last few decades. The key point of PNG is to drive the LOS angular rate to zero to guide the missile to intercept the target with zero miss distance. However, because of the terrible disturbance resulting from target maneuvers, environment noise, and measurement error, PNG cannot provide the qualified performance in some extreme cases. For example, for missiles with maneuvering targets, such as interceptors or air-to-air missiles, the LOS angular rate usually varies with the target maneuvers; this variation always results in perturbations that PNG or argument PNG cannot cope with. Hence, it is necessary to design a novel robust guidance law to resist this perturbation.

With the development of the modern control theory in recent years, many scholars proposed many advanced guidance laws for intercepting maneuvering targets. To cite some typical works, to attenuate the effect of bounded uncertain and unknown interference, Yang and Chen [6] proposed a robust H-infinity guidance law by regarding unpredictable target maneuvers as bounded unknowns. Based on the results of their research, Liu and Shen [7] presented a novel three-dimensional spherical H-infinity guidance law that takes missile acceleration constraints into account. By formulating interception as a nonlinear perturbation attenuation H-infinity problem, Yang and Chen [8] presented a novel robust guidance law. Zhou et al. [9]

presented a L_2 gain performance guidance law with the aid of a Lyapunov-like approach. In the work of Yan and Ji [10], a novel input-to-state stability-based guidance (ISSG) law was proposed to limit bounded target maneuvers and estimate the bounded LOS angular rate. In addition to the mentioned guidance laws and their variants, SMC-based guidance laws are alternatives to the most popular guidance laws because of their inherent strong robustness and FTC properties.

Second-order SMC is a useful method to allow guided missiles to intercept maneuvering targets with the desired impact angles. Because of its robustness, global convergence, and order reduction, the sliding mode controller has drawn great attention from research communities and has been used in a variety of applications in various fields, such as missile guidance, autopilots of unmanned air vehicles (UAV), robotic manipulator control, and microelectromechanical system (MEMS) gyroscopes [11–14]. Based on the SMC theory, many advanced guidance laws were coined for maneuvering targets. For example, by using the SMC technique, Zhou et al. [15] proposed a novel FTC guidance law to guide the LOS angular rate to converge to zero or within a small neighborhood of zero in finite time. Facing planar interception, Moon et al. [16] provided an adaptive sliding mode guidance approach based on the reaching law, in which the key point is that the convergent rate should increase in proportion to the decrease in the distance between the missile and the target. By using the so-called inertial delay control (IDC) technique to estimate the target acceleration, Phadke and Talole [17] proposed an SMC-based PN guidance law that requires no knowledge of the bounds of the target acceleration. Kumar et al. [18] proposed a planar nonsingular terminal sliding mode guidance law in the presence of impact angle constraints; however, they did not consider the FTC property.

For a LOS angle constrained maneuvering target interception, some challenges should be taken into account. First, the knowledge of a LOS angle is difficult to be obtained, especially when the target is moving with a large velocity and a large acceleration. Next, in real practice, the properties of the actuator, such as the response rate and efficiency margin, are another two important factors which also should be taken into consideration. In addition, some perturbations such as measurement error and environmental noise may result in performance degradation. Considering these problems, this paper discusses a new nonsingular continuous impact-angle-constraint SMC guidance law that forces the system state to converge to a sliding manifold in finite time as well as drives the sliding manifold to converge to zero in finite time. By using a switchable design of the sliding manifold, this control approach avoids the singularity that a conventional TSM can encounter. Furthermore, this guidance law utilizes the STA algorithm to reduce the chattering phenomenon. Moreover, a 2-OB which can track the unknown trajectory is employed to estimate the target maneuvers. Combining with the proposed observer and guidance algorithm, the LOS angle error (the difference between the desired LOS angle and the real LOS angle) and LOS angular rate can converge to zero in finite time.

The rest of this paper is organized as follows: the planar and spherical mathematical model of the engagement phase is provided, and the guidance strategy is discussed in Section 2; the 2-OB and the finite-time convergent guidance approach is proposed in Section 3; some simulation results are given and discussed in Section 4; a brief conclusion of this paper is given in Section 5; some proofs of the proposed propositions are given in Appendices A, B, and III.

2. Problem Formulation

2.1. Planar Mathematical Model of the Engagement Phase. Throughout the paper, the research object is assumed to satisfy the following hypothesizes: (i) the mass of the missile is in uniform distribution, (ii) the no roll or roll rate is small enough, and (iii) the mechanical properties of the missile are similar in every direction perpendicular to the roll axis. As a result, the missile can be regarded as a point mass. To simplify the problem, the relationship between the missile and the target during the engagement phase can be taken into account as a planar interception, which is illustrated in Figure 1.

From Figure 1, one can conclude that

$$\dot{r} = V_T \cos(\gamma_T - \lambda) - V_M \cos(\gamma_M - \lambda), \tag{1}$$

$$\dot{\lambda} = \frac{[V_T \sin(\gamma_T - \lambda) - V_M \cos(\gamma_M - \lambda)]}{r}, \tag{2}$$

$$\dot{\gamma}_M = \frac{a_M}{V_M}, \tag{3}$$

$$\dot{\gamma}_T = \frac{a_T}{V_T}, \tag{4}$$

where M denotes the missile and T denotes the target; V_T and V_M denote the velocities of the target and the missile, respectively; a_T and a_M denote the accelerations of the target and the missile, respectively; r and $\dot{r}$ denote the distance and its derivative, respectively, between the missile and the target; λ and $\dot{\lambda}$ denote the LOS angle and the LOS angular rate, respectively; γ_M and $\dot{\gamma}_M$ denote the heading angle and the heading angular rate of the missile, respectively; γ_T and $\dot{\gamma}_T$ denote the heading angle and the heading angular rate of the target, respectively.

Taking the derivative of equation (1) and equation (2) with respect to time yields

$$\ddot{r} = r\dot{\lambda}^2 + a_{Tr} - a_{Mr}, \tag{5}$$

$$\ddot{\lambda} = -\frac{2\dot{r}\dot{\lambda}}{r} + \frac{a_{T\lambda}}{r} - \frac{a_{M\lambda}}{r}. \tag{6}$$

Here, $a_{Tr} = a_T \sin(\lambda - \gamma_T)$ and $a_{Mr} = a_M \sin(\lambda - \gamma_M)$ denote accelerations following the LOS direction of the target and the missile, respectively. $a_{T\lambda} = a_T \cos(\lambda - \gamma_T)$ and $a_{M\lambda} = a_M \cos(\lambda - \gamma_M)$ denote accelerations perpendicular to the LOS direction of the target and the missile, respectively. This completes the planar mathematical model.

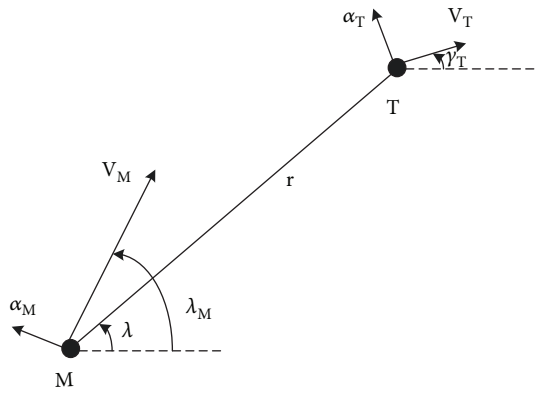

Figure 1: The planar model of the relationship between the missile and the target.

Remark 1. For a missile controlled by active forces, equation (5) and equation (6) must be considered simultaneously during the process of guidance law design. However, for a missile only controlled by aerodynamic forces, the velocity in the LOS direction can be regard as constant. Hence, using only equation (6) to design the guidance law is adequate.

2.2. Strategy of Interception. According to the zeroing LOS angular rate principle, assuming that the LOS angular rate will converge to zero when collision occurs, from equation (2), one can infer that

$$V_T \sin\left(\gamma_{Tf} - \lambda_f\right) = V_M \sin\left(\gamma_{Mf} - \lambda_f\right), \tag{7}$$

where the subscript f denotes the values of the relevant parameters at terminal time.

Denote impact angle θ_{imp} as the following equation:

$$\theta_{\text{imp}} = \gamma_{Tf} - \gamma_{Mf}. \tag{8}$$

Substituting equation (8) into equation (7) yields

$$V_T \sin\left(\gamma_{Tf} - \lambda_f\right) - V_M \sin\left(\gamma_{Tf} - \theta_{\text{imp}} - \lambda_f\right) = 0. \tag{9}$$

By assuming that $V_T < V_M$, solving equation (9) yields

$$\lambda_f = \gamma_{Tf} - \tan^{-1}\left(\frac{\sin\theta_{\text{imp}}}{\cos\theta_{\text{imp}} - V_T/V_M}\right). \tag{10}$$

From equation (10), one can conclude that, for any given impact angle θ_{imp}, there must exist one and one only relevant LOS angle. In other words, the problem of impact angle constraints can be transformed as the tracking LOS angle problem. We can design a Lyapunov approach to drive the LOS angle λ to converge to the desired LOS angle λ_d and the LOS angular rate $\dot{\lambda}$ to converge to zero in finite time to solve this problem.

2.3. Some Assumptions and Lemmas. The following assumptions and lemmas are used throughout this paper.

Assumption 1. There must exist a minimum distance $r_{\min}$ between the missile and the target. For any given r, the following is required: $|r| \geq r_{\min}$.

Remark 3. Because of the length of the missile and the length of the target from the shells to the point masses, Assumption 1 is reasonable.

Assumption 2. Because of the physical limits, the target maneuvers are unknown but continuous and bounded.

Assumption 3. Actuators can respond to guidance commands in real time.

Assumption 4. The vertical acceleration of a missile afforded by actuators is no more than 300 m/s^2.

Lemma 1 [19]. *Suppose that $V(x)$ is a C^1 smoothing positive function defined on $U \in \mathbb{R}^n$. For any parameters $\beta_1 > 0$ and $\beta_2 \in (0, 1)$, if there always exists a function defined on $U \in \mathbb{R}^n$ that satisfies*

$$\dot{V}(x) + \beta_1 V^{\beta_2}(x) \leq 0, \tag{11}$$

then there must exist a region $U_0 \in \mathbb{R}^n$ such that any $V(x)$ that starts from $U_0 \in \mathbb{R}^n$ will approach to $V(x) \equiv 0$ in finite time T_{reach}. Moreover, this time T_{reach} is governed by

$$T_{\text{reach}} \leq \frac{V^{1-\beta_2}(x_0)}{\beta_1(1-\beta_2)}, \tag{12}$$

where $V(x_0)$ is the initial value of $V(x)$.

Lemma 2 [20]. *Suppose a function can be described as*

$$f(x) = x^T A x, \tag{13}$$

where $x = [x_1, x_2, \cdots, x_n]^T \in \mathbb{R}^n$ and A is a positive definite nonsingular matrix that is radially unbounded. The proposed function $f(x)$ satisfies

$$\lambda_{\min}(A)\|x\|^2 \leq f(x) \leq \lambda_{\max}(A)\|x\|^2, \tag{14}$$

where $\lambda_{\min}(A)$ and $\lambda_{\max}(A)$ denote the minimum and the maximum eigenvalues, respectively. Moreover, $\|x\| = \sqrt{x^T x} \in R$ is the Euclid norm.

Lemma 3 [21]. *For any given $x \in \mathbb{R}$ and $y \in \mathbb{R}$, with $c > 0$ and $d > 0$, the following is satisfied:*

$$|x|^c |y|^d \leq \frac{c}{c+d}|x|^{c+d} + \frac{d}{c+d}|x|^{c+d}. \tag{15}$$

Lemma 4 [22]. *Consider a cascaded system which is formulated as*

$$\begin{aligned} \dot{x}_1 &= f(t, x_1, x_2) = f_1(t, x_1) + g(t, x_1, x_2), \\ \dot{x}_2 &= f_2(t, x_2), \end{aligned} \tag{16}$$

where $x_1 \in \mathbb{R}^n$, $x_2 \in \mathbb{R}^m$, $f_1(t, x_1) = f(t, x_1, 0)$, *and* $g(t, x_1, x_2) = f(t, x_1, x_2) - f(t, x_1, 0)$. *Assume that the subsystems* $\dot{x}_1 = f_1(t, x_1)$ *and* $\dot{x}_2 = f_2(t, x_2)$ *are uniformly globally finite-time stable (UGFTS). For arbitrary-fixed and bounded* x_2, *if there exists a positive definite FTB function* $B(t, x_1)$: $\mathbb{R}_{\geq 0} \times \mathbb{R}^n \to \mathbb{R}_{\geq 0}$, *which satisfies* $B(t, x_1)|_{(4)} \leq \beta_6(B(t, x_1))$, $\forall t \geq t_0 \geq 0$, *where* β_6 : $\mathbb{R}_{\geq 0} \to \mathbb{R}_{\geq 0}$ *is a nondecreasing function satisfying* $\beta_6(a) \geq 0$ *and* $\int_a^\infty 1/\beta_6(s)ds = \infty$ *for some constant* $a > 0$, *cascaded system (16) is UGFTS.*

3. Guidance Law Design and Stability Analysis

3.1. 2-OB Design and Stability Analysis. According to Assumption 2, the acceleration of the target is unknown. To estimate the target acceleration, based on second-order SMC theory, an observer is proposed as follows:

$$\begin{aligned} \dot{\widehat{q}} &= \dot{\widehat{a}}_{T\lambda} + h_1 |q - \widehat{q}|^{1-1/\upsilon} \operatorname{sign}(q - \widehat{q}) - \dot{r}\dot{\lambda} - a_{M\lambda}, \\ \dot{\widehat{a}}_{T\lambda} &= h_2 |q - \widehat{q}|^{1-2/\upsilon} \operatorname{sign}(q - \widehat{q}), \end{aligned} \tag{17}$$

where $q = r\dot{\lambda}$, $h_1 > 0$, $h_2 > 0$, and $\upsilon > 2$ are the design parameters; $\widehat{q}$ and $\widehat{a}_{T\lambda}$ are the estimated values of q and $a_{T\lambda}$, respectively.

Proposition 1. *Considering system equations (1)–(4) and observer equation (17), the estimated errors denoted as* $e_1 = q - \widehat{q}$ *and* $e_2 = a_{T\lambda} - \widehat{a}_{T\lambda}$ *will approach the following area in finite time:*

$$\|e\| \leq \left(\frac{\dot{a}_{T\lambda}^{\max} \|B\|}{\lambda_{\min}(M)} \right)^{(\upsilon-1)/(\upsilon-2)}, \tag{18}$$

where $e = [e_1, e_2]^T$ *and*

$$\begin{aligned} M &= \begin{bmatrix} h_1 h_2 + h_1^3 \dfrac{\upsilon - 1}{\upsilon} & -h_1^2 \dfrac{\upsilon - 1}{\upsilon} \\ -h_1^2 \dfrac{\upsilon - 1}{\upsilon} & h_1 \dfrac{\upsilon - 1}{\upsilon} \end{bmatrix}, \\ B &= [-h_1, 2]^T. \end{aligned} \tag{19}$$

$\lambda_{\min}(M)$ *is denoted as the minimum eigenvalue of matrix* M; *similarly,* $\lambda_{\max}(M)$ *is denoted as the maximum eigenvalue of matrix* M.

Proof of Proposition 1. See Appendix A.

3.2. Sliding Manifold Design. By denoting $\varepsilon_1 = \lambda - \lambda_d$ and $\varepsilon_2 = \dot{\lambda} - \dot{\lambda}_d = \dot{\lambda}$, a novel nonsingular switchable sliding manifold is presented as

$$s = \varepsilon_2 + k_1 \varepsilon_1 + k_2 \alpha(\varepsilon_1), \tag{20}$$

where $k_1 > 0$ and $k_2 > 0$ are the design parameters and $\alpha(x_1)$ is governed by

$$\alpha(\varepsilon_1) = \begin{cases} |\varepsilon_1|^{\tau_1/\tau_2} \operatorname{sign}(\varepsilon_1), & \text{if } \bar{s} = 0 \text{ or } \bar{s} \neq 0, |\varepsilon_1| \geq \mu, \\ b_1 \varepsilon_1 + b_2 \operatorname{sign}(\varepsilon_1) \varepsilon_1^2, & \text{if } \bar{s} \neq 0, |\varepsilon_1| < \mu, \end{cases} \tag{21}$$

with $b_1 = (2 - \tau_1/\tau_2)\mu^{\tau_1/\tau_2 - 1}$, $b_2 = (2 - \tau_1/\tau_2)\mu^{\tau_1/\tau_2 - 2}$, and $\bar{s} = \varepsilon_2 + k_1\varepsilon_1 + k_2|\varepsilon_1|^{p/q} \operatorname{sign}(\varepsilon_1)$. τ_1 is an even integer, τ_2 is an even integer, μ is a very small constant, and sign $(\cdot)$ denotes the sigmoid function, which is governed by

$$\operatorname{sign}(x) = \begin{cases} -1, & \text{if } x < 0, \\ 0, & \text{if } x = 0, \\ 1, & \text{if } x > 0. \end{cases} \tag{22}$$

$$\bar{s} = \varepsilon_1 + k^{-q/p} \varepsilon_2^{q/p}, \tag{23}$$

where parameter k is a positive constant.

Remark 4. The design parameters b_1 and b_2 are properly selected according to the above discussion such that the switching manifold equation (20) is continuous and differentiable.

Remark 5. Note that to avoid singularity, this switching manifold will switch to a novel linear sliding mode (LSM) switching manifold when the system state ε_1 is very small and the conventional fast terminal sliding mode (TSM) switching manifold is not equal to zero [23]. In addition to this switching manifold, another nonlinear terminal sliding mode (NTSM) switching manifold is governed by [24].

Remark 6. In comparison with the conventional NTSM switching manifold equation (22), the proposed switching manifold uses a switchable design technique to avoid the singularity phenomenon. When the system trajectory is close to zero, the switching manifold will switch from the terminal switching manifold to the linear switching manifold. Moreover, when the system trajectory is far away from the switching manifold, the linear term $k_1\varepsilon_1$ will accelerate the convergent rate and the nonlinear term $k_2\alpha(\varepsilon_1)$ will play a leading role. Hence, compared with the conventional NTSM switching manifold equation (22), the proposed switching manifold shows better convergent performance if the parameters are properly selected.

Proposition 2. *For an arbitrary second-order certain system (such as system equation (6)) or uncertain system, if the proposed NTSM switching manifold* $s = 0$ *is achieved, then the system states* ε_1 *and* ε_2 *will converge to zero in finite time.*

Proof of Proposition 2. See Appendix B.

3.3. Finite-Time Convergent Guidance Law Design. Taking the derivative of equation (19) with respect to time yields

$$\dot{s} = \dot{\varepsilon}_2 + k_1\varepsilon_2 + k_2\dot{\alpha}(\varepsilon_1), \tag{24}$$

where the third term $\dot{\alpha}(\varepsilon_1)$ is governed by

$$\dot{\alpha}(\varepsilon_1) = \begin{cases} (p/q)\varepsilon_1^{p/q-1}\varepsilon_2, & \text{if } \bar{s} = 0 \text{ or } \bar{s} \neq 0, |\varepsilon_1| \geq \mu, \\ b_1\varepsilon_2 + 2b_2 \text{ sign } (\varepsilon_1)\varepsilon_1\varepsilon_2, & \text{if } \bar{s} \neq 0, |\varepsilon_1| < \mu. \end{cases} \tag{25}$$

For the convenience of following research, equation (20) can be rewritten as

$$\dot{s}(\varepsilon_1, \varepsilon_2, t) = f(\varepsilon_1, \varepsilon_2, t) + b(\varepsilon_1, \varepsilon_2, t)a_{M\lambda}, \tag{26}$$

with

$$f(\varepsilon_1, \varepsilon_2, t) = \left\{ \begin{array}{ll} \dfrac{-2\dot{r}\dot{\lambda}/r + a_{T\lambda}}{r + k_1\dot{\varepsilon} + k_2(p/q)\varepsilon_1^{p/q-1}\varepsilon_2}, & \text{if } \bar{s} = 0 \text{ or } \bar{s} \neq 0, |\varepsilon_1| \geq \mu \\ \dfrac{-2\dot{r}\dot{\lambda}/r + a_{T\lambda}}{r + k_1\dot{\varepsilon} + k_2(b_1\varepsilon_2 + 2b_2 \text{ sign } (\varepsilon_1)\varepsilon_1\varepsilon_2)}, & \text{if } \bar{s} \neq 0, |\varepsilon_1| < \mu \end{array} \right\}, \tag{27}$$

$$b(\varepsilon_1, \varepsilon_2, t) = \frac{-1}{r}.$$

By replacing $a_{T\lambda}$ with $\hat{a}_{T\lambda}$, the estimated state function

$$\hat{f}(\varepsilon_1, \varepsilon_2, t) = \left\{ \begin{array}{ll} \dfrac{-2\dot{r}\dot{\lambda}/r + \hat{a}_{T\lambda}}{r + k_1\dot{\varepsilon} + k_2(p/q)\varepsilon_1^{p/q-1}\varepsilon_2}, & \text{if } \bar{s} = 0 \text{ or } \bar{s} \neq 0, |\varepsilon_1| \geq \mu \\ \dfrac{-2\dot{r}\dot{\lambda}/r + \hat{a}_{T\lambda}}{r + k_1\dot{\varepsilon} + k_2(b_1\varepsilon_2 + 2b_2 \text{ sign } (\varepsilon_1)\varepsilon_1\varepsilon_2)}, & \text{if } \bar{s} \neq 0, |\varepsilon_1| < \mu \end{array} \right\}. \tag{28}$$

$\hat{f}(\varepsilon_1, \varepsilon_2, t)$ can be described as

The proposed switchable controller can be described as

$$\begin{aligned} a_{M\lambda} &= -b^{-1}(\varepsilon_1, \varepsilon_2, t)\left(\hat{f}(\varepsilon_1, \varepsilon_2, t) + c_1|s|^{1-1/\gamma} \text{ sign } (s) - c_2\varsigma\right), \\ \dot{\varsigma} &= b(\varepsilon_1, \varepsilon_2, t)|s|^{1-2/\gamma} \text{ sign } (s), \end{aligned} \tag{29}$$

where c_1 and c_2 are positive constants and $\gamma > 2$ is a constant.

Proposition 3. *Considering the proposed second-order system equation (16), the proposed controller equation (28) can drive the system states to converge to the switching manifold in finite time.*

Proof of Proposition 3. For an "observer-controller" system, the conventional separation principle is not reasonable. The proof should be divided into two steps. The system's boundedness will be illustrated via the FTB [22] function method in Step I, and the feature FTC of the LOS angular rate will be illustrated in Step II.

Step I. Substituting equation (29) into equation (26) yields

$$\dot{s} = \frac{a_{T\lambda} - \hat{a}_{T\lambda}}{r} - \frac{k_1}{r}|s|^{1-1/\gamma} \text{ sign } (s) - \frac{k_2}{r}\int \frac{|s|^{1-2/\gamma} \text{ sign } (s)}{r} dt. \tag{30}$$

For simplicity, denote two auxiliary variables as

$$\begin{aligned} \omega_1 &= s, \\ \omega_2 &= a_{T\lambda} - \hat{a}_{T\lambda} - k_2\int \frac{|s|^{1-2/\gamma} \text{ sign } (s)}{r} dt. \end{aligned} \tag{31}$$

Taking the derivatives of equation (31) with respect to time yields

$$\begin{aligned}\dot{\omega}_1 &= \frac{\omega_2}{r} - \frac{k_1}{r}|\omega_1|^{1-1/\gamma}\ \text{sign}\ (\omega_1),\\ \dot{\omega}_2 &= \dot{a}_{T\lambda} - \dot{\hat{a}}_{T\lambda} - \frac{k_2}{r}|\omega_2|^{1-2/\gamma}\ \text{sign}\ (\omega_1).\end{aligned} \tag{32}$$

Denoting the auxiliary vector $\omega = [|\omega_1|^{1-1/\gamma}\ \text{sign}\ (\omega_1), \omega_2]^T$ and taking the following FTB function into account yield:

$$V_1 = \omega^T\omega = |\omega_1|^{2(\gamma-1)/\gamma} + \omega_2^2. \tag{33}$$

It is easy to verify that $V_1 \in \mathbb{R}^2$ is continuous within its domain of definition, except for the set $\Psi = \{(\omega_1, \omega_2) \in \mathbb{R}^2 | \omega_1 = 0\}$. However, it follows from $\omega_1 = 0$ and $\omega_2 \neq 0$ that $\dot{\omega}_1 = \omega_2 \neq 0$ and the trajectories of system states will pass through Ψ rather than stay in, until system states reach zero. Thus, the proposed Lyapunov function V_1 can be used to verify the property of FTB of the proposed guidance.

Taking the time derivative of V_1 yields

$$\begin{aligned}\dot{V}_1 &= 2\frac{\gamma-1}{\gamma}|\omega_1|^{1-2/\gamma}\ \text{sign}\ (\omega_1)\left(\frac{\omega_2}{r} - \frac{k_1}{r}|\omega_1|^{1-1/\gamma}\ \text{sign}\ (\omega_1)\right)\\ &\quad + 2\omega_2\left(\dot{a}_{T\lambda} - \dot{\hat{a}}_{T\lambda} - \frac{k_2}{r}|\omega_1|^{1-2/\gamma}\ \text{sign}\ (\omega_1)\right)\\ &\leq 2\frac{\gamma-1}{\gamma}|\omega_1|^{1-2/\gamma}\ \text{sign}\ (\omega_1)\frac{\omega_2}{r}\\ &\quad + 2\omega_2\left(\dot{a}_{T\lambda} - \dot{\hat{a}}_{T\lambda} - \frac{k_2}{r}|\omega_1|^{1-2/\gamma}\ \text{sign}\ (\omega_1)\right)\\ &\leq 2\frac{\gamma-1}{\gamma}|\omega_1|^{1-2/\gamma}\ \text{sign}\ (\omega_1)\frac{|\omega_2|}{r} + 2|\omega_2|\left|\dot{a}_{T\lambda} - \dot{\hat{a}}_{T\lambda}\right|\\ &\quad + 2\frac{k_2}{r}|\omega_1|^{1-2/\gamma}|\omega_2| \leq 2\frac{\gamma-1}{\gamma}|\omega_1|^{1-2/\gamma}\ \text{sign}\ (\omega_1)\frac{|\omega_2|}{r_{\min}}\\ &\quad + 2|\omega_2|\left|\dot{a}_{T\lambda} - \dot{\hat{a}}_{T\lambda}\right| + 2\frac{k_2}{r_{\min}}|\omega_1|^{1-2/\gamma}|\omega_2|.\end{aligned} \tag{34}$$

According to Lemma 3 and the average value of the inequality, one can conclude that

$$\begin{aligned}\dot{V}_1 &\leq 2\frac{\gamma-1}{\gamma r_{\min}}\left(\frac{\gamma-2}{2\gamma-2}|\omega_1|^{2(\gamma-1)/\gamma} + \frac{\gamma}{2\gamma-2}|\omega_2|^{2(\gamma-1)/\gamma}\right)\\ &\quad + |\omega_2|^2 + \left|\dot{a}_{T\lambda} - \dot{\hat{a}}_{T\lambda}\right|^2 + 2\frac{k_2}{\gamma r_{\min}}\left(\frac{\gamma-2}{2\gamma-2}|\omega_1|^{2(\gamma-1)/\gamma}\right.\\ &\quad \left. + \frac{\gamma}{2\gamma-2}|\omega_2|^{2(\gamma-1)/\gamma}\right).\end{aligned} \tag{35}$$

Consider the following two cases.

Case 1. If $|\omega_2| \leq 1$ is satisfied, it follows from $2(\gamma-1)/\gamma \in (1, 2)$ that $|\omega_2|^{2(\gamma-1)/\gamma} \leq |\omega_2|^2$. Substituting this inequality into equation (30) yields

$$\begin{aligned}\dot{V}_1 &\leq \frac{1}{r_{\min}}\left(\frac{\gamma-2}{\gamma} + \frac{k_2(\gamma-2)}{\gamma}\right)|\omega_1|^{2(p-1)/p}\\ &\quad + \left(1 + \frac{1}{r_{\min}}\left(1 + \frac{k_2\gamma}{\gamma-1}\right)\right)|\omega_2|^2 + \left|\dot{a}_{T\lambda} - \dot{\hat{a}}_{T\lambda}\right|^2\\ &\leq K_1V_1 + \left|\dot{a}_{T\lambda} - \dot{\hat{a}}_{T\lambda}\right|^2,\end{aligned} \tag{36}$$

with $K_1 = \max\{(1/r_{\min})((\gamma-2/\gamma) + (k_2(\gamma-2)/\gamma-1)), 1 + (1/r_{\min})(k_2\gamma/\gamma-1)\}$.

Case 2. If $|\omega_2| \geq 1$ is satisfied, it follows from $2(\gamma-1)/\gamma \in (1, 2)$ that $|\omega_2|^{2(\gamma-1)/\gamma} \leq 1$. Substituting this inequality into equation (34) yields

$$\begin{aligned}\dot{V}_1 &\leq \frac{1}{r_{\min}}\left(\frac{\gamma-2}{\gamma} + \frac{k_2(\gamma-2)}{\gamma}\right)|\omega_1|^{2(p-1)/p}\\ &\quad + \left(1 + \frac{1}{r_{\min}}\left(1 + \frac{k_2\gamma}{\gamma-1}\right)\right)\\ &\quad + |\omega_2|^2 + \left|\dot{a}_{T\lambda} - \dot{\hat{a}}_{T\lambda}\right|^2\\ &\leq K_2V_1 + \frac{1}{r_{\min}}\left(1 + \frac{k_2\gamma}{\gamma-1}\right) + \left|\dot{a}_{T\lambda} - \dot{\hat{a}}_{T\lambda}\right|^2,\end{aligned} \tag{37}$$

with $K_1 = \max\{(1/r_{\min})((\gamma-2/\gamma) + (k_2(\gamma-2)/\gamma-1)), 1\}$.

According to Proposition 1, $|\dot{a}_{T\lambda} - \dot{\hat{a}}_{T\lambda}|$ is globally bounded. In other words, there exists a positive constant κ that satisfies $|\dot{a}_{T\lambda} - \dot{\hat{a}}_{T\lambda}| \leq \kappa$. Combined with the results of Case 1 and Case 2, one can conclude that

$$\dot{V}_1 \leq KV_1 + L, \tag{38}$$

where $K = \max\{K_1, K_2\}$ and $L = (1/r_{\min})(1 + (k_2\gamma/\gamma-1)) + \kappa^2$.

Hence, in any time range of $[0, t]$, solving inequality (35) yields

$$V_1 \leq \left(V_1(0) + \frac{L}{K}\right)e^{Kt} - \frac{L}{K}, \tag{39}$$

where $V_1(0)$ denotes the initial value of V_1. This completes the proof of the boundedness of the system.

Step II. According to Lemma 1, the estimated target acceleration $\hat{a}_{T\lambda}$ will converge into a small region around the real target acceleration $\dot{\hat{a}}_{T\lambda}$ in finite time. Hence, equation (32) can be rewritten as

$$\begin{aligned}\dot{\omega}_1 &= \frac{\omega_2}{r} - \frac{k_1}{r}|\omega_1|^{1-1/\gamma}\ \text{sign}\ (\omega_1),\\ \dot{\omega}_2 &= -\frac{k_2}{r}|\omega_2|^{1-2/\gamma}\ \text{sign}\ (\omega_1).\end{aligned} \tag{40}$$

To prove the finite-time stability, the selected Lyapunov function is governed by

$$V_2 = \frac{c_2\gamma}{\gamma-1}|\omega_1|^{2(1-1/\gamma)} + \frac{1}{2}\omega_2^2 + \frac{1}{2}\left(k_1|\omega_1|^{(1-1/\gamma)}\,\text{sign}\,(\omega_1) - \omega_2\right)^2. \tag{41}$$

Similar to V_1, V_2 is continuous except for $\Psi = \{(\omega_1, \omega_2) \in \mathbb{R}^2 | \omega_1 = 0\}$ and can be used to verify the property of FTC.

Taking the derivative of equation (32) with respect to time yields

$$\dot{V}_2 = -|\omega_1|^{-1/\gamma}\left(c_1c_2|\omega_1|^{2(\gamma-1)/\gamma} + \frac{\gamma-1}{\gamma}c_1^3|\omega_1|^{2(\gamma-1)/\gamma} - 2\frac{\gamma-1}{\gamma}c_1^2|\omega_1|^{(\gamma-1)/\gamma}\,\text{sign}\,(\omega_1)\omega_2 + \frac{\gamma-1}{\gamma}c_1\omega_2^2\right). \tag{42}$$

Equation (42) can be rewritten as

$$\dot{V}_2 = -|\omega_1|^{-1/\gamma}\omega^T P\omega, \tag{43}$$

with

$$P = \begin{bmatrix} c_1c_2 + c_1^3\dfrac{\gamma-1}{\gamma} & -c_1^2\dfrac{\gamma-1}{\gamma} \\ -c_1^2\dfrac{\gamma-1}{\gamma} & c_1\dfrac{\gamma-1}{\gamma} \end{bmatrix}. \tag{44}$$

Since parameters c_1 and c_2 are positive constants and $\gamma > 2$, it is easy to verify that matrix P is positive definite.

Equation (41) can be rewritten as

$$V_2 = \omega^T Q\omega, \tag{45}$$

with

$$Q = \frac{1}{2}\begin{bmatrix} \dfrac{c_2\gamma}{\gamma-1} + c_1^2 & -c_1 \\ -c_1 & 2 \end{bmatrix}. \tag{46}$$

Since c_1 and c_2 are positive constants and $\gamma > 2$, it is easy to verify that matrix Q is positive definite and radial unbounded. According to Lemma 2, one can obtain

$$\lambda_{\min}(Q)\|\omega\|^2 \le V_2 \le \lambda_{\max}(Q)\|\omega\|^2. \tag{47}$$

Table 1: Values of the design parameters.

Parameter	k_1	k_2	c_1	c_2	h_1	h_2	γ	υ	μ
Value	5	5	600	500	300	200	2.1	2.5	0.3

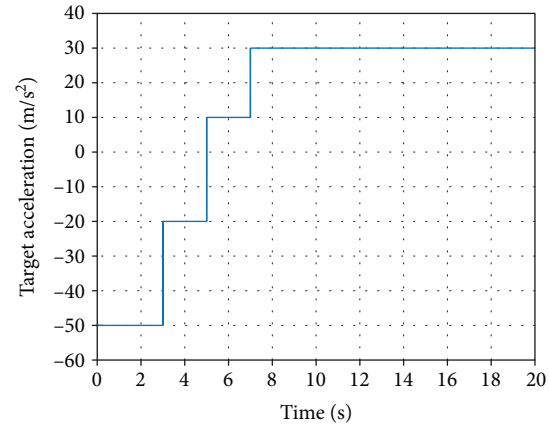

Figure 2: The target maneuver in case 3.

It follows from $\|\omega\| = \sqrt{|\omega_1|^{2(\gamma-1)/\gamma} + \omega_2^2} \ge |\omega_1|^{(\gamma-1)/r}$ that $|\omega_1|^{1/\gamma} \ge \|\omega\|^{-1/(\gamma-1)}$. Combining equation (43) and equation (45), one can conclude that

$$\begin{aligned} \dot{V}_2 &\le -\|\omega\|^{-1/(\gamma-1)}\lambda_{\min}(P)\|\omega\|^2 \\ &\le -\lambda_{\min}(P)\|\omega\|^{(2\gamma-3)/(\gamma-1)} \\ &\le -\frac{\lambda_{\min}(P)}{[\lambda_{\max}(Q)]^{(2\gamma-3)/(2\gamma-2)}}V_2^{(2\gamma-3)/(2\gamma-2)}. \end{aligned} \tag{48}$$

Since $(2\gamma-3)/(2\gamma-2) \in (0, 0.5)$, according to Lemma 1, the system states of equation (6) can converge to zero in finite time. This completes the proof.

Remark 7. A FTB function of system equation (6) and observer equation (17) with a certain upper bound is presented in Step I, and the UGFTS property of the proposed guidance law is demonstrated in Step II. From Assumption 2, one can imply that the observer is UGFTS. Finally, according to Lemma 4, system equation (6) with observer equation (17) and controller equation (29) is UGFTS.

4. Case Study

In this section, numerical simulations are performed to demonstrate efficiency and effectiveness of the proposed guidance law for missiles that intercept three types of targets during terminal guidance. The simulations are performed with the MATLAB platform by using the fourth-order Runge-Kutta solver with a fixed step size of 0.001 s.

4.1. Simulation Setup. Verify the effectiveness of the proposed guidance law in the presence of a two-dimension environment. The required initial conditions are selected as follows: (1) the initial range is $r(0) = 7071$ m, (2) target velocity is

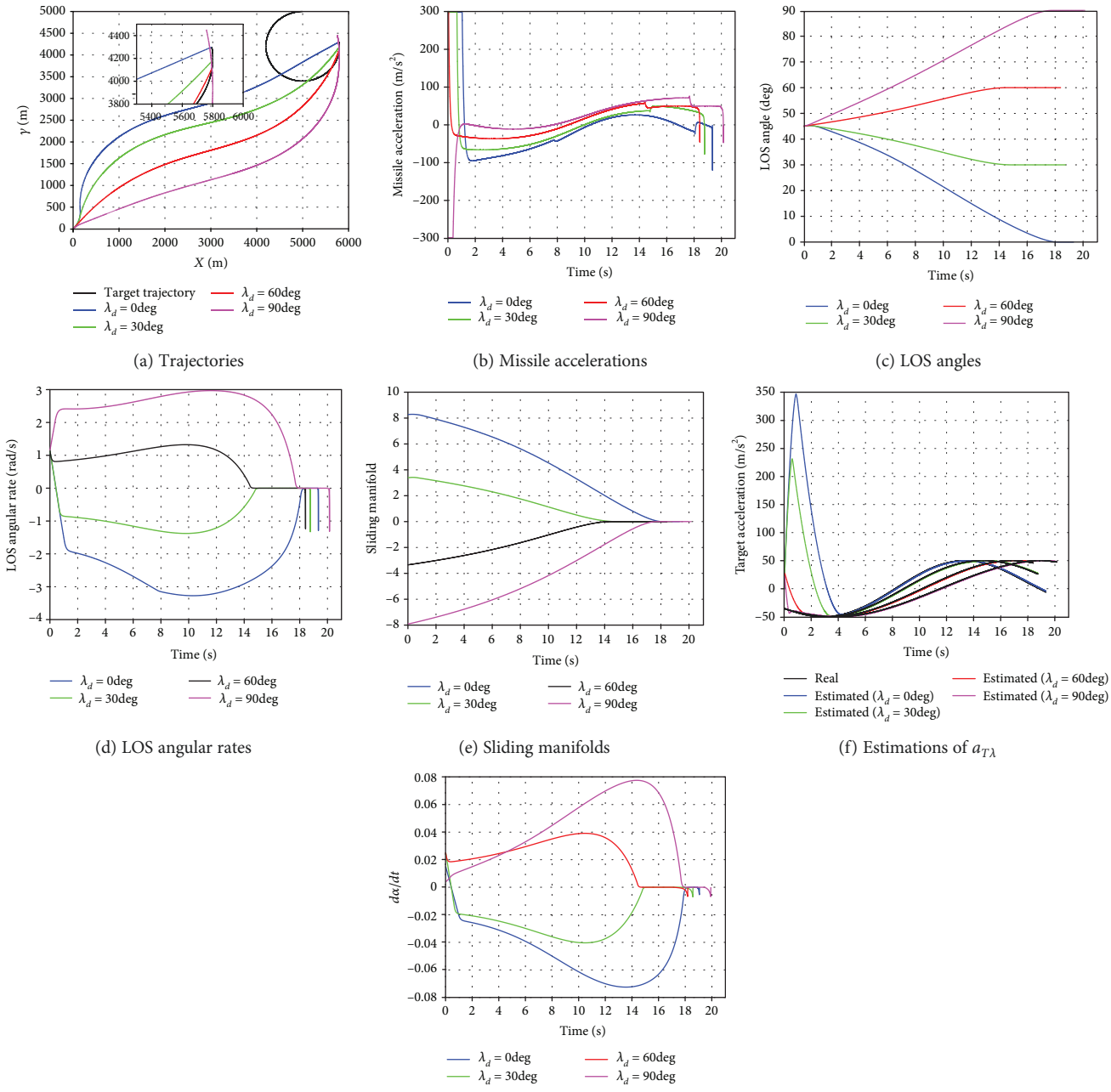

(a) Trajectories

(b) Missile accelerations

(c) LOS angles

(d) LOS angular rates

(e) Sliding manifolds

(f) Estimations of $a_{T\lambda}$

(g) The third term in equation (24)

FIGURE 3: Simulation results of case 1.

$V_T = 200$ m/s, (3) interceptor velocity is $V_M = 400$ m/s, (4) initial LOS angle is $\lambda(0) = 45$ deg, (5) initial heading angle of the missile is $\gamma_M(0) = 45$ deg, (6) initial heading angle of the target is $\gamma_T(0) = 180$ deg, and (7) values of the design parameters are given in Table 1.

4.2. Simulation Results. Verify the effectiveness of the proposed guidance law in the presence of a two-dimension environment. To strengthen the universality of the proposed planar guidance law, three performances of the target maneuvers are considered, as described in the following: case 1: the target maneuver is constant, $a_T = 50$ m/s^2, case 2: the target maneuver satisfies the sinusoidal components, $a_T = 50 \sin(0.5t)$ m/s^2, and case 3: the target maneuver is random, as illustrated in Figure 2.

The simulation results include trajectories of the missile and the target, missile accelerations, LOS angles and angular rates, sliding manifolds, and estimated target maneuvers. Figure 3 is for case 1, Figure 4 is for case 2, and Figure 5 is for case 3. As shown in Figures 3(a), 4(a), and 5(a), one can see clearly that the missile can intercept the target accurately in the presence of different target maneuvers and different impact angles under the proposed guidance law. In Figures 3(b), 4(b), and 5(b), the missile accelerations are limited to 300 m/s^2 and are chattering free. Figures 3(c), 4(c), and 5(c) and Figures 3(d), 4(d), and 5(d) imply that

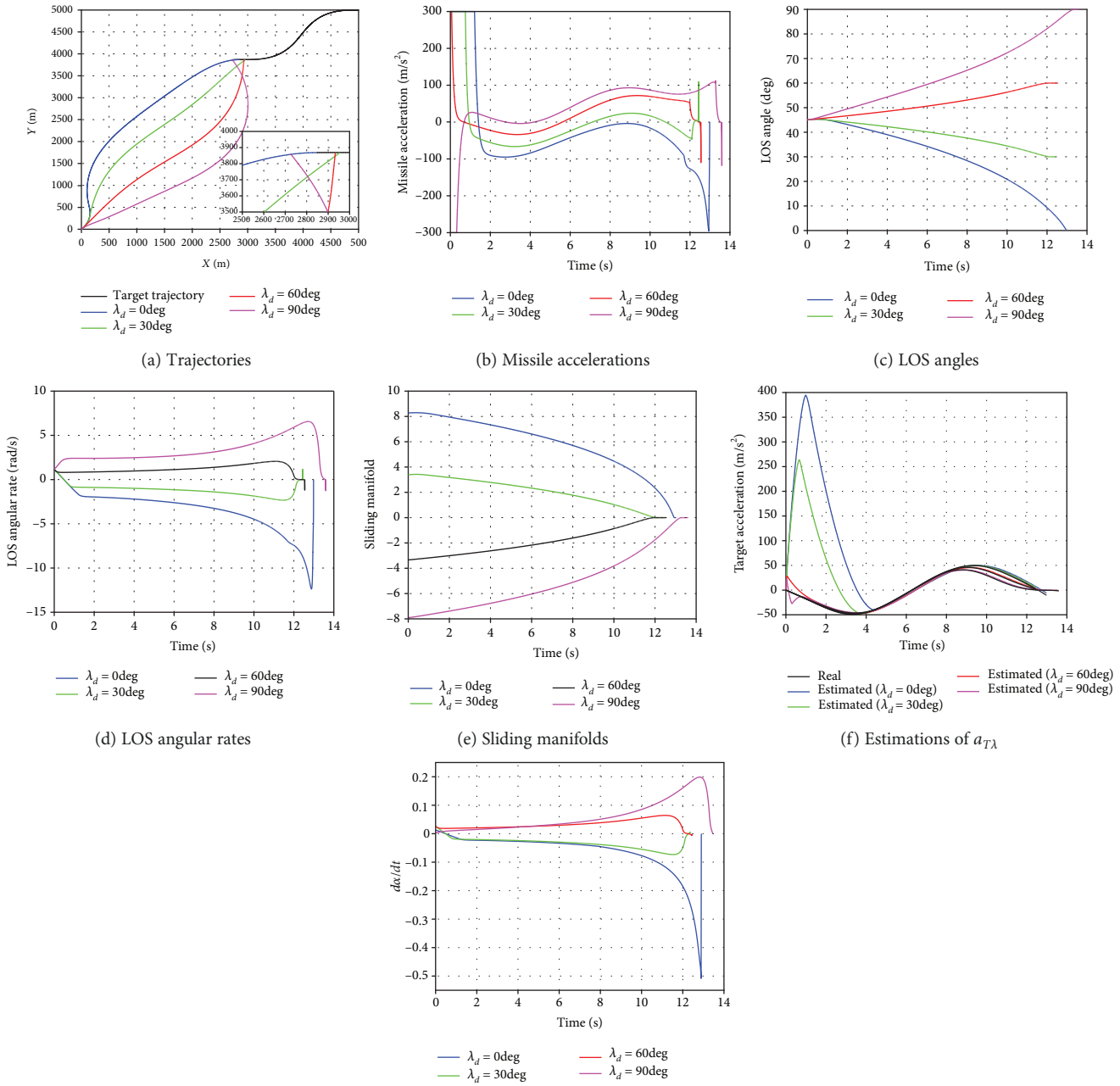

(a) Trajectories

(b) Missile accelerations

(c) LOS angles

(d) LOS angular rates

(e) Sliding manifolds

(f) Estimations of $a_{T\lambda}$

(g) The third term in equation (24)

FIGURE 4: Simulation results of case 2.

the LOS angles converge to the desired values at terminal time and the LOS angular rates converge to zero at terminal time. Figures 3(e), 4(e), and 5(e) give the curves of the sliding manifolds. Figures 3(f), 4(f), and 5(f) show the real values of the unknowns and their estimated values; clearly, every estimated value will reach to the related real value and sliding on its surface. Figures 3(g), 4(g), and 5(g) depict the third terms of equation (24). These results verify the efficiency and effectiveness of the proposed planar guidance law.

Note that there exists a divergent phenomenon in some figures, such as in Figures 4(d) and 5(d). This phenomenon results from the inherent property of guidance. When the interceptor is very close to the target, r is very small or even regarded as zero. Considering that r is contained in denominators in the system of equation (6), the terrible influence from $r \to 0$ is difficult to affect. However, by considering that r has a minimum value $r_{\min}$ (Assumption 1), the divergent phenomenon at the end of the engagement phase can be ignored; thus, the proposed guidance law still meets the requirements in actual practice.

Next, for the purpose of further demonstration of the efficiency and effectiveness of the proposed guidance law,

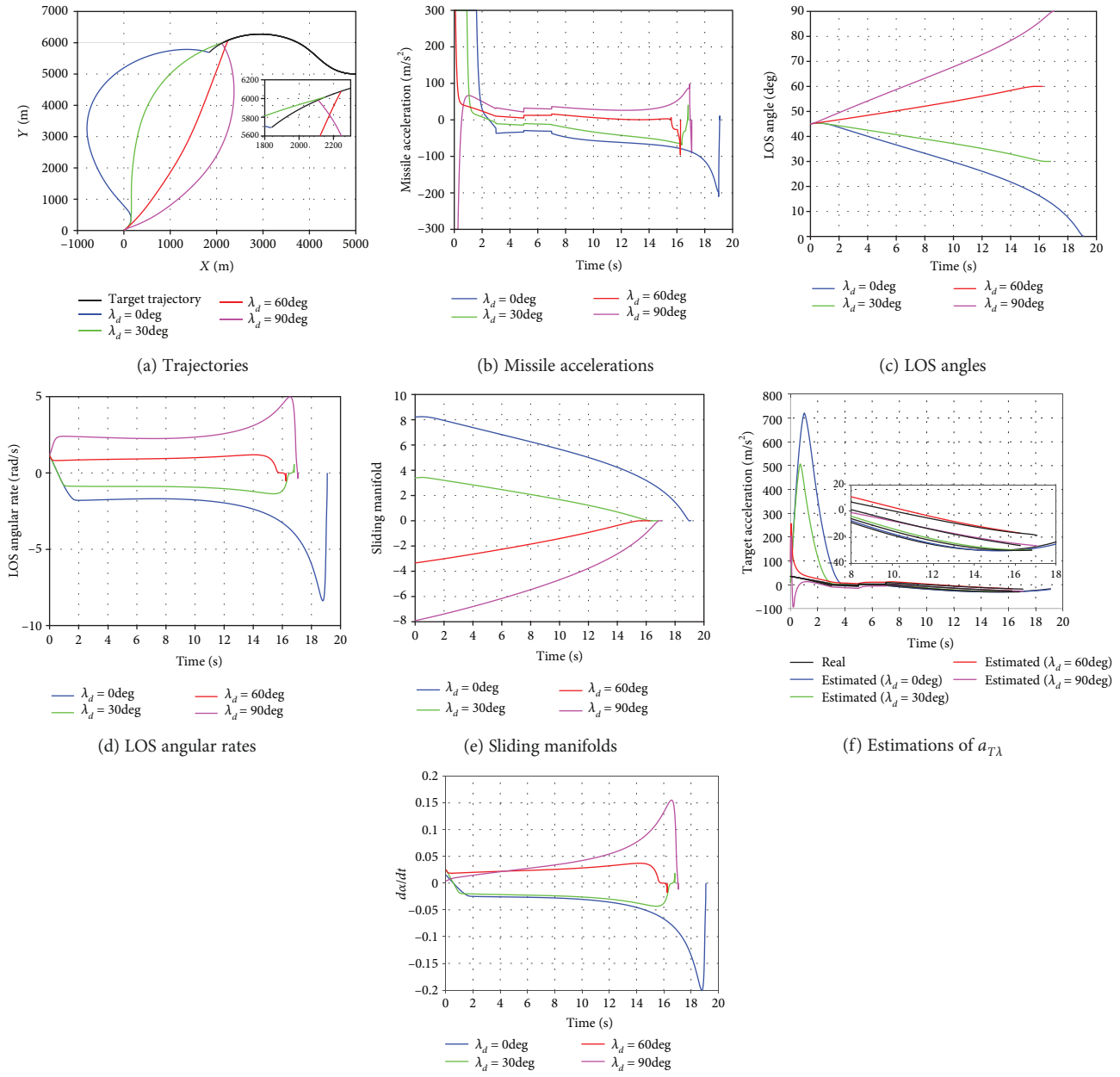

(a) Trajectories

(b) Missile accelerations

(c) LOS angles

(d) LOS angular rates

(e) Sliding manifolds

(f) Estimations of $a_{T\lambda}$

(g) The third term in equation (24)

Figure 5: Simulation results of case 3.

the NTSM guidance law in [20] shown below is employed for comparison:

$$\begin{aligned} a_{M\lambda} &= -2\dot{r}\dot{\lambda} + \frac{r\beta}{\alpha}|e_2|^{2-\alpha}\,\mathrm{sign}\,(e_2) \\ &\quad + d + \nu_1|\bar{s}|^{1-1/p}\,\mathrm{sign}\,(\bar{s}) + \nu_2\xi, \\ \dot{\xi} &= \frac{|e_2|^{\alpha-1}|\bar{s}|^{1-2/p}}{r}\,\mathrm{sign}\,(\bar{s}), \\ \bar{s} &= e_1 + \frac{1}{\beta}|e_2|^{\alpha}\,\mathrm{sign}\,(e_2), \\ d &= a_M + a_{T\lambda} - a_{M\lambda}. \end{aligned} \tag{49}$$

Here, assume that knowledge of the target acceleration $a_{T\lambda}$ in the NTSM guidance law can be obtained in real time. Moreover, the design parameters α, β, p, ν_1, and ν_2 are chosen to be the same as those in [22]. In this comparison case, the target maneuver is chosen as $a_T = -50\sin(0.5t)$ m/s^2 and the desired final LOS angles are selected as $\lambda_d = 30$ deg and $\lambda_d = 60$ deg.

The simulation results of the comparison are illustrated in Figure 6. Similar to the above simulation cases, Figures 6(a) and 6(b) demonstrate that the missile intercepts the target with high accuracy and that the actuator can provide enough acceleration during the engagement phase. Figures 6(c) and 6(d) show the superiority of the proposed

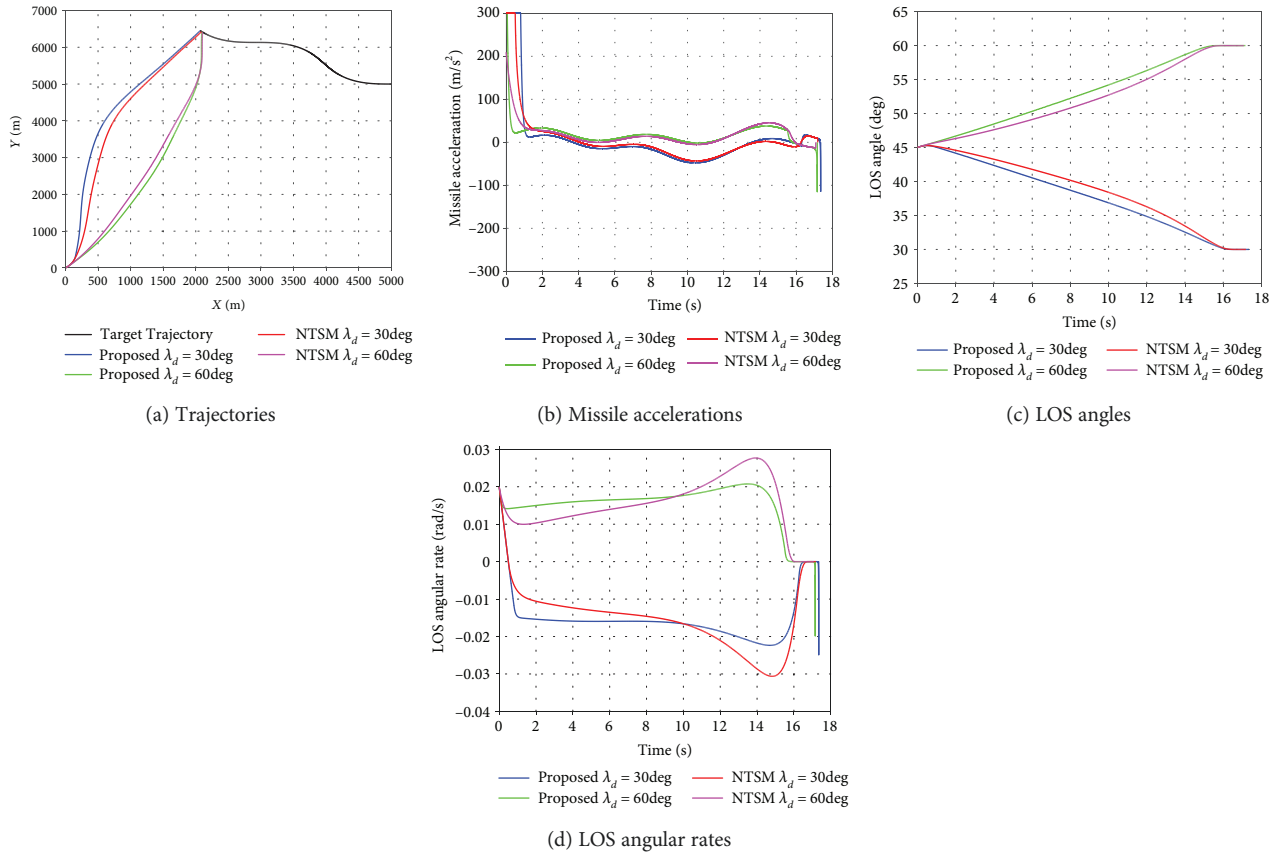

(a) Trajectories

(b) Missile accelerations

(c) LOS angles

(d) LOS angular rates

Figure 6: Simulation results of comparison.

guidance law. Although the two guidance laws can drive the LOS angle and its rate to converge on their desired values, the proposed guidance law achieves this goal more quickly in the presence of the same design parameters. This result verifies Remark 6.

Remark 8. In real practice, considering that the central processing units (CPUs) on the interceptors can only identify and generate simple instant signal, it is important to design discrete-time guidance laws [25]. Compared with the continuous sliding mode guidance law, however, the chattering phenomenon is much easier to occur and much more difficult to avoid. Thanks to the works in [26, 27], this problem has been addressed.

5. Conclusion

This paper presented a chattering-free nonsingular finite-time convergent guidance law in the presence of impact angle constraints; more specifically, the target maneuvers are obtained by proposing a second-order SMC-based observer and singularity is avoided by proposing a switchable sliding manifold. A super twisting type of guidance law was proposed to force the LOS angle and angular rate to converge to the desired values in finite time. Furthermore, the proposed planar guidance was extended in three-dimension cases. Numerical simulation results demonstrated the aforementioned properties.

Appendix

A

Proof of Proposition 1. By denoting $q = r\dot{\lambda}$, equation (6) can be rewritten as

$$\dot{q} = -\dot{r}\dot{\lambda} + a_{T\lambda} - a_{M\lambda}. \tag{A.1}$$

Substituting equation (A.1) into equation (17) yields

$$\begin{aligned} \dot{e}_1 &= e_2 - h_1 |e_1|^{1-1/\upsilon} \operatorname{sign}(e_1), \\ \dot{e}_2 &= \dot{a}_{T\lambda} - h_2 |e_1|^{1-2/\upsilon} \operatorname{sign}(e_1). \end{aligned} \tag{A.2}$$

Regarding system equation (17), consider the following Lyapunov function:

$$V_3 = \frac{h_2 \upsilon}{\upsilon - 1} |e_1|^{2(\upsilon-1)/\upsilon} + \frac{1}{2} e_2^2 + \frac{1}{2} \left(h_1 |e_1|^{(\upsilon-2)/\upsilon} \operatorname{sign}(e_1) - e_2 \right)^2. \tag{A.3}$$

Equation (A.3) can be rewritten in the following form:

$$V_3 = e^T \Lambda e, \tag{A.4}$$

with

$$\Lambda = \frac{1}{2}\begin{bmatrix} \frac{h_2 \upsilon}{\upsilon - 1} + h_1^2 & -h_1 \\ -h_1 & 2 \end{bmatrix}. \tag{A.5}$$

Because $h_2 > 0$ and $\upsilon > 2$, V_3 is positive and unbounded in the radial direction. According to Lemma 2,

$$\lambda_{\min}(\Lambda)\|e\|^2 \le V_3 \le \lambda_{\min}(\Lambda)\|e\|^2. \tag{A.6}$$

Note that V_3 is continuous, except $\Psi = \{(\omega_1, \omega_2) \in \mathbb{R}^2 | \omega_1 = 0\}$. Similar to V_1, V_3 can be used to evaluate the stability of system equation (43). Taking the derivative with respect to time yields

$$\begin{aligned} \dot{V}_3 &= \left(\frac{h_2 \upsilon}{\upsilon - 1} + \frac{1}{2}h_1^2\right)\frac{2\upsilon - 2}{\upsilon}|e_1|^{(\upsilon-2)/\upsilon}\,\mathrm{sign}\,(e_1) \\ &\quad \cdot \left(e_2 - h_1|e_1|^{1-1/\upsilon}\,\mathrm{sign}\,(e_1)\right) \\ &\quad + \left(2e_2 - h_1|e_1|^{(\upsilon-1)/\upsilon}\,\mathrm{sign}\,(e_1)\right) \\ &\quad \cdot \left(\dot{a}_{T\lambda} - h_2|e_1|^{(\upsilon-2)/\upsilon}\,\mathrm{sign}\,(e_1)\right) \\ &\quad - h_1\frac{\upsilon - 1}{\upsilon}|e_1|^{-1/\upsilon}e_2\left(e_2 - h_1|e_1|^{1-1/\upsilon}\,\mathrm{sign}\,(e_1)\right) \\ &= -|e_1|^{-1/\upsilon}\left(h_1 h_2|e_1|^{2(\upsilon-1)/\upsilon} + \frac{\upsilon - 1}{\upsilon}h_1^3|e_1|^{2(\upsilon-1)/\upsilon}\right. \\ &\quad \left. - 2\frac{\upsilon - 1}{\upsilon}h_1^2|e_1|^{(\upsilon-1)/\upsilon}\,\mathrm{sign}\,(e_1)e_2 + \frac{\upsilon - 1}{\upsilon}h_1 e_2^2\right) \\ &\quad + \left(2e_2 - h_1|e_1|^{2(\upsilon-1)/\upsilon}\,\mathrm{sign}\,(e_1)\right)\dot{a}_{T\lambda} \\ &\le -|e_1|^{-1/p}e^T M e + \dot{a}_{T\lambda}^{\max} B e. \end{aligned} \tag{A.7}$$

Because $h_1 > 0$, $h_2 > 0$, and $\upsilon > 2$, it is easy to verify that M is Hurwitz.

It follows from $\|e\| = \sqrt{|e_1|^{2(\upsilon-1)/\upsilon} + e_2^2} \ge |e_1|^{(\upsilon-1)/\upsilon}$ that

$$|e_1|^{-1/\upsilon} \ge \|e\|^{-1/(\upsilon-1)}. \tag{A.8}$$

Combined with equation (A.6), equation (A.7), and equation (A.8), one can imply that

$$\begin{aligned} \dot{V}_1 &\le -|e_1|^{-1/\upsilon}\lambda_{\min}(M)\|e\|^2 + \dot{a}_{T\lambda}^{\max}\|B\|\|e\| \\ &\le -\left(\lambda_{\min}(M)\|e\|^{(\upsilon-2)/(\upsilon-1)} - \dot{a}_{T\lambda}^{\max}\|B\|\right)\|e\| \\ &\le -\left(\lambda_{\min}(M)\|e\|^{(\upsilon-2)/(\upsilon-1)} - \dot{a}_{T\lambda}^{\max}\|B\|\right)\frac{V_1^{1/2}}{\sqrt{\lambda_{\max}(\Lambda)}}. \end{aligned} \tag{A.9}$$

If $\lambda_{\min}(M)\|e\|^{(\upsilon-2)/(\upsilon-1)} - \dot{a}_{T\lambda}^{\max}\|B\| > 0$, equation (A.9) can be transformed as

$$\dot{V}_1 \le -\frac{\beta V_1^{1/2}}{\sqrt{\lambda_{\max}(\Lambda)}}, \tag{A.10}$$

where $\beta = \lambda_{\min}(M)\|e\|^{(\upsilon-2)/(\upsilon-1)} - \dot{a}_{T\lambda}^{\max}\|B\| > 0$. According to Lemma 1, system equation (43) will converge into the following region:

$$\|e\| \le \left(\frac{\dot{a}_{T\lambda}^{\max}\|B\|}{\lambda_{\min}(M)}\right)^{(\upsilon-1)/(\upsilon-2)}. \tag{A.11}$$

This completes the proof.

B

Proof of Proposition 2. It follows from $s = 0$ that $\varepsilon_2 = -k_1\varepsilon - k_2\varepsilon^{\tau_1/\tau_2}$. Considering a Lyapunov function $V_1(\varepsilon) = \varepsilon_1^2/2$, its derivative with respect to time is described as

$$\begin{aligned} \dot{V}_1(\varepsilon) &= \varepsilon_1\varepsilon_2 = -k_1\varepsilon_1^2 - k_2\varepsilon^{(\tau_1+\tau_2)/\tau_2} \\ &= -2k_1 V_1 - 2^{(\tau_1+\tau_2)/2\tau_2}k_2 V_1^{(\tau_1+\tau_2)/2\tau_2}. \end{aligned} \tag{B.1}$$

According to Lemma 1 and $(\tau_1/\tau_2 + 1)/2 \in (0.75, 1)$, one can imply that $\varepsilon_1 = 0$ must be achieved in finite time. Moreover, from equation (19), if $s = 0$ and $\varepsilon_1 = 0$ can be obtained in finite time, then one can also imply that $\varepsilon_2 = 0$ can be achieved in finite time. This completes the proof.

Data Availability

The readers can access the data from part 4 of this article. The authors declare that all data is available.

Conflicts of Interest

The authors declare that they have no conflicts of interest.

Acknowledgments

The National Natural Science Foundation of China (Grant no. 61172182 and Grant U1613225) supported this work.

References

[1] Z. Yang, H. Wang, D. Lin, and L. Zang, "A new impact time and angle control guidance law for stationary and nonmaneuvering targets," *International Journal of Aerospace Engineering*, vol. 2016, Article ID 6136178, 14 pages, 2016.

[2] A. Budiyono and H. Rachman, "Proportional guidance and CDM control synthesis for a short-range homing surface-to-air missile," *Journal of Aerospace Engineering*, vol. 25, no. 2, pp. 168–177, 2012.

[3] F. W. Nesline and P. Zarchan, "A new look at classical vs modern homing missile guidance," *Journal of Guidance, Control, and Dynamics*, vol. 4, no. 1, pp. 78–85, 1981.

[4] P. Zarchan, *Tactical and Strategic Missile Guidance*, American Institute of Aeronautics and Astronautics Publications, New York, 1998.

[5] S. A. Murtaugh and H. E. Criel, "Fundamentals of proportional navigation," *IEEE Spectrum*, vol. 3, no. 12, pp. 75–85, 1966.

[6] C. D. Yang and H. Y. Chen, "Three-dimensional nonlinear H_∞ guidance law," *International Journal of Robust and Nonlinear Control*, vol. 11, no. 2, pp. 109–129, 2001.

[7] L. J. Liu and Y. Shen, "Three-dimension H_∞ guidance law and capture region analysis," *IEEE Transactions on Aerospace and Electronic Systems*, vol. 48, no. 1, pp. 419–429, 2012.

[8] C. D. Yang and H. Y. Chen, "Nonlinear H robust guidance law for homing missiles," *Journal of Guidance, Control, and Dynamics*, vol. 21, no. 6, pp. 882–890, 1998.

[9] D. Zhou, C. Mu, and T. Shen, "Robust guidance law with L_2 gain performance," *Transactions of the Japan Society for Aeronautical and Space Sciences*, vol. 44, no. 144, pp. 82–88, 2001.

[10] H. Yan and H. B. Ji, "Guidance laws based on input-to-state stability and high-gain observers," *IEEE Transactions on Aerospace and Electronic Systems*, vol. 48, no. 3, pp. 2518–2529, 2012.

[11] H. Du, S. Li, and C. Qian, "Finite-time attitude tracking control of spacecraft with application to attitude synchronization," *IEEE Transactions on Automatic Control*, vol. 56, no. 11, pp. 2711–2717, 2011.

[12] S. Wang and J. Fei, "Robust adaptive sliding mode control of MEMS gyroscope using T–S fuzzy model," *Nonlinear Dynamics*, vol. 77, no. 1-2, pp. 361–371, 2014.

[13] S. He and D. Lin, "A robust impact angle constraint guidance law with seeker's field-of-view limit," *Transactions of the Institute of Measurement and Control*, vol. 37, no. 3, pp. 317–328, 2015.

[14] L. W. Zhao and C. C. Hua, "Finite-time consensus tracking of second-order multi-agent systems via nonsingular TSM," *Nonlinear Dynamics*, vol. 75, no. 1-2, pp. 311–318, 2014.

[15] D. Zhou, S. Sun, and K. L. Teo, "Guidance laws with finite time convergence," *Journal of Guidance, Control, and Dynamics*, vol. 32, no. 6, pp. 1838–1846, 2009.

[16] J. Moon, K. Kim, and Y. Kim, "Design of missile guidance law via variable structure control," *Journal of Guidance, Control, and Dynamics*, vol. 24, no. 4, pp. 659–664, 2001.

[17] S. B. Phadke and S. E. Talole, "Sliding mode and inertial delay control based missile guidance," *IEEE Transactions on Aerospace and Electronic Systems*, vol. 48, no. 4, pp. 3331–3346, 2012.

[18] S. R. Kumar, S. Rao, and D. Ghose, "Sliding-mode guidance and control for all-aspect interceptors with terminal angle constraints," *Journal of Guidance, Control, and Dynamics*, vol. 35, no. 4, pp. 1230–1246, 2012.

[19] S. P. Bhat and D. S. Bernstein, "Finite-time stability of continuous autonomous systems," *SIAM Journal on Control and Optimization*, vol. 38, no. 3, pp. 751–766, 2000.

[20] Y. Ji, D. Lin, W. Wang, and S. Lin, "Finite-time convergent guidance law based on second-order sliding mode control theory," *International Journal of Aeronautical and Space Sciences*, vol. 18, no. 4, pp. 697–708, 2017.

[21] C. Qian and W. Lin, "A continuous feedback approach to global strong stabilization of nonlinear systems," *IEEE Transactions on Automatic Control*, vol. 46, no. 7, pp. 1061–1079, 2001.

[22] S. Li and Y. P. Tian, "Finite-time stability of cascaded time-varying systems," *International Journal of Control*, vol. 80, no. 4, pp. 646–657, 2007.

[23] S. He, D. Lin, and J. Wang, "Chattering-free adaptive fast convergent terminal sliding mode controllers for position tracking of robotic manipulators," *Proceedings of the Institution of Mechanical Engineers, Part C: Journal of Mechanical Engineering Science*, vol. 230, no. 4, pp. 514–526, 2016.

[24] S. He, D. Lin, and J. Wang, "Continuous second-order sliding mode based impact angle guidance law," *Aerospace Science and Technology*, vol. 41, pp. 199–208, 2015.

[25] S. He, W. Wang, and J. Wang, "Discrete-time super-twisting guidance law with actuator faults consideration," *Asian Journal of Control*, vol. 19, no. 5, pp. 1854–1861, 2017.

[26] H. Du, X. Yu, M. Z. Q. Chen, and S. Li, "Chattering-free discrete-time sliding mode control," *Automatica*, vol. 68, pp. 87–91, 2016.

[27] H. Du, X. Chen, G. Wen, X. Yu, and J. Lu, "Discrete-time fast terminal sliding mode control for permanent magnet linear motor," *IEEE Transactions on Industrial Electronics*, vol. 68, no. 6, pp. 87–91, 2016.